15th World Congress on Computational Mechanics (WCCM-XV)
8th Asian Pacific Congress on Computational Mechanics (APCOM-VIII)
Virtual Congress: 31 July – 5 August 2022
S. Koshizuka (Ed.)

# SURROGATE MODEL OF ELASTIC LARGE-DEFORMATION BEHAVIORS OF COMPLIANT MECHANISM USING CO-ROTATIONAL BEAM ELEMENT

**KAI SUTO[1], YUSUKE SAKAI[2], KOTARO TANIMICHI[1] AND TAISUKE OHSHIMA[1]**

[1] Nature Architects, Inc.
Tokyo 107-0052, Japan
info@nature-architects.com

[2] Sony Computer Science Laboratories, Inc. Kyoto Laboratory
Kyoto 600-8086, Japan
Yusuke.C.Sakai@sony.com

**Key words:** Compliant mechanism, Large-deformation analysis, Surrogate model, Co-rotational beam element

**Abstract.** *We propose a surrogate model for predicting in-plane nonlinear structural deformations of a compliant mechanism. Our model utilizing a 2-dimensional co-rotational beam element extracts the essential deformation degrees-of-freedoms (DOFs) of bending flexible beams. The total number of DOFs of nodes at both ends of a 2-dimensional beam is six, while the number of deformation DOFs is three, i.e., axial extension, symmetric bending, and anti-symmetric bending. Therefore, it enables us to reduce the computational cost, from six to three, associated with the models by using the essential deformation DOFs of the co-rotational beam element. Moreover, it is difficult to predict the nonlinear responses of forces derived from displacements of a compliant mechanism due to bifurcation of the deformation-path. To overcome the problem, we generate the datasets by applying external forces and use the inverse response for constructing the surrogate models. In the numerical example, large-deformation behaviors of several types of compliant mechanisms are predicted by our surrogate models constructed by three typical learning algorithms: polynomial approximation, radial basis function, and neural network. The prediction performances and computational costs are investigated for verifying that they can be beneficial tools for designing a compliant mechanism with nonlinear elastic deformation behaviors.*

## 1 INTRODUCTION

In a wide range of engineering fields, mechanical design problems crucially affect the total performance of a product. In particular, designing a largely deformable structure is not a simple task due to its geometrical nonlinearities. We traditionally design the structure with desirable deformation DOFs by rigid-body mechanism, which is composed of rigid links and additional joints such as pin and roller. While compliant mechanism can realize the desirable motions by the designers by utilizing elastic deformation of each flexible member [1]. Compliant mechanisms have opened new avenues for the design and fabrication of structures with complex deformation DOFs. Following Ref.[1], there are two main advantages of using compliant mechanisms: (i) cost reduction and (ii) increased mechanical performance for precise deformations. The former advantage leads to fabricating them monolithically. It contributes to reducing the number of additional parts such as rotating and sliding joints, and it is possible to generate

a lightweight structure rather than a rigid-body mechanism. The latter leads to reducing the errors and damages due to backlash and friction of joints. However, there have been some difficulties in broadening compliant mechanisms to general applications. Design of them is still hard for many designers, because the sophisticated knowledge and techniques of computational modeling and analysis are required due to their complex geometrical configurations and specific deformation behaviors. Moreover, numerical simulation with geometrical nonlinearities can be a time-consuming task.

Pseudo-rigid-body model is often used for describing the large-deformation behaviors of a compliant mechanism [1]. A basic idea of the pseudo-rigid-body model is based on a simple analyzing system for reducing the deformation DOFs by using a combination of rigid bars and torsional springs, and it is also associated with the rigid-body mechanism theory. However, it is necessary to construct a computational model based on the geometrical shape of each structure by trial and error.

A data-driven approach can improve the simplicity of the design process of complex structures with highly nonlinear deformation behaviors [2, 3]. Recent advances in data-driven approaches to design structures have shown superior effectiveness for predictions of their mechanical properties. There have been many developments for a surrogate model predicting elastic large-deformation behaviors of a compliant mechanism. Malomo *et al.* [2] proposed FlexMaps, which allow us to carry out fast and accurate numerical simulation for large-deformation of a compliant mechanism. The idea of their method is that they utilize the bending beam model, with the stiffness matrix constructed by the datasets of the nonlinear structural responses of a compliant mechanism, as an equivalent model to the original structure. Papadopoulos *et al.* [3] predict the nonlinear deformation behaviors of a carbon nanotube by using the surrogate model, which has the essential deformation DOFs, constructed by the scattered datasets collected by finite-element simulations. A data-driven approach enables us to propose a method for obtaining nonlinear deformations of a compliant mechanism without resort to sophisticated techniques required for designing a complex geometrical configuration.

In this paper, we propose a surrogate model for predicting in-plane nonlinear structural deformation behaviors of a compliant mechanism composed of multiple bending beams. The basic idea of our surrogate model as briefly illustrated in Fig. 1 is that the use of an equivalent beam model with reduced deformation DOFs overcomes the computational task caused by a complex geometrical configuration and large DOFs of detail model composed of multiple beams. Our surrogate model is constructed by the following three steps: (i) preparing a structural component, with essential deformation DOFs, that is appropriate for being incorporated into the numerical simulations based on finite-element analysis, (ii) carrying out finite-element analysis with geometrical nonlinearities for sampling the datasets of static structural responses of detail model composed of multiple beams, and (iii) learning the datasets for predicting the nonlinear structural responses of a compliant mechanism. At step (i), we use a 2-dimensional co-rotational beam element, which enables us to separate the DOFs into rigid and natural straining modes. By using the co-rotational beam element with essential deformation DOFs corresponding to the natural straining modes, the computational costs associated with dimensions of datasets can be reduced from six to three. The datasets collected by numerical simulation at step (ii) are stress-strain relationships derived from the natural straining modes of a co-rotational beam element. Our surrogate models are based on three learning algorithms: polynomial approximation, radial basis function, and neural network. In the numerical example, we investigate the prediction performances of our models and compare the computational costs and deformations with those of the detail models composed of multiple bending beams.

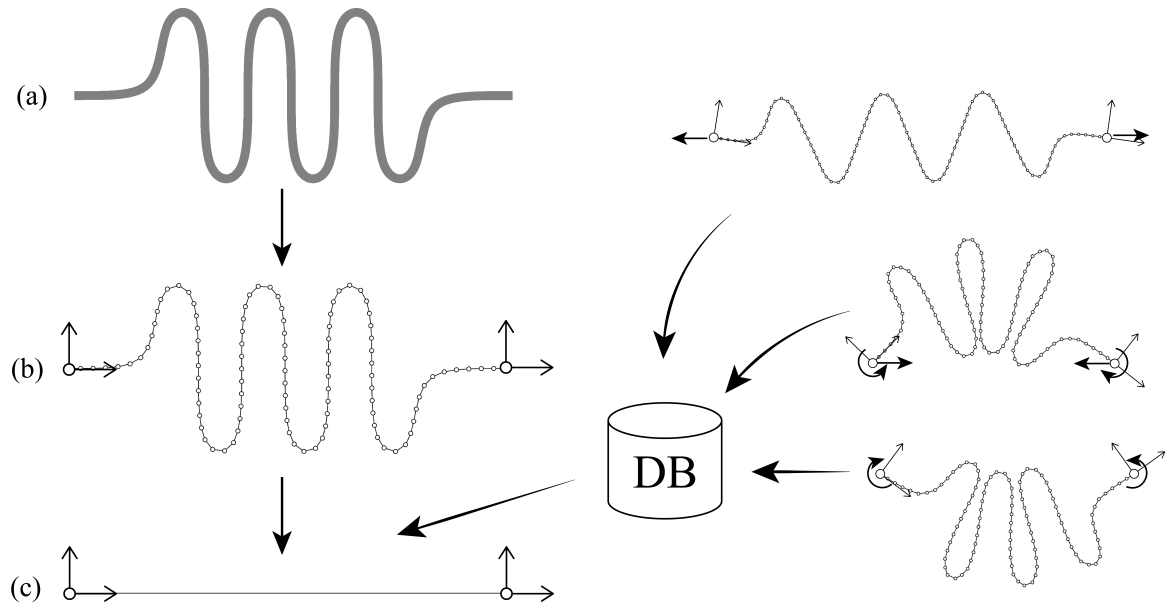


**Figure 1**: Conversion of a compliant mechanism; (a) continuous model, (b) discretized detail model composed of bending beams incorporated into numerical simulation by finite-element analysis, (c) equivalent model composed of a single co-rotational beam element based on a surrogate model constructed by the scattered datasets of nonlinear structural responses.

## 2 2-DIMENSIONAL CO-ROTATIONAL BEAM ELEMENT

Consider a 2-dimensional bending beam—Euler-Bernoulli beam—composed of two end nodes. The DOFs on each node of a beam are three: two translations and one rotation; accordingly, the total number of DOFs is determined as six for a single beam element. To reduce the DOFs, we use a 2-dimensional co-rotational beam element as explained in Ref. [4]. Figure 2 illustrates the deformation modes of a 2-dimensional beam element. By introducing the idea of a co-rotational beam element, the deformation mode of a beam can be separated into two parts: rigid body mode and natural straining mode. The rigid body mode is composed of translation and rotation as illustrated in Fig. 2(b). While, the three strains of the natural straining mode: axial extension, symmetric bending, and anti-symmetric bending, as illustrated in Figs. 2(c)–(e), are represented as $\mathbf{v} = [u, \varphi_s, \varphi_a]^{\mathrm{T}}$. The generalized forces corresponding to $\mathbf{v}$ are introduced by $\mathbf{t} = [N, M_s, M_a]^{\mathrm{T}}$.

The equivalent beam model with the nonlinear response between $\mathbf{v}$ and $\mathbf{t}$ [3] can be implemented into the computational procedure that we deal with global coordinate displacements $\mathbf{p}_g$ and forces $\mathbf{q}_g$ obtained by carrying out the following two coordinate transformations: (i) between the element and co-rotational coordinate systems and (ii) between the co-rotational and global coordinate systems.

The transformations from displacements $\mathbf{p}_e$ and forces $\mathbf{q}_e$ in the element coordinate system to those in

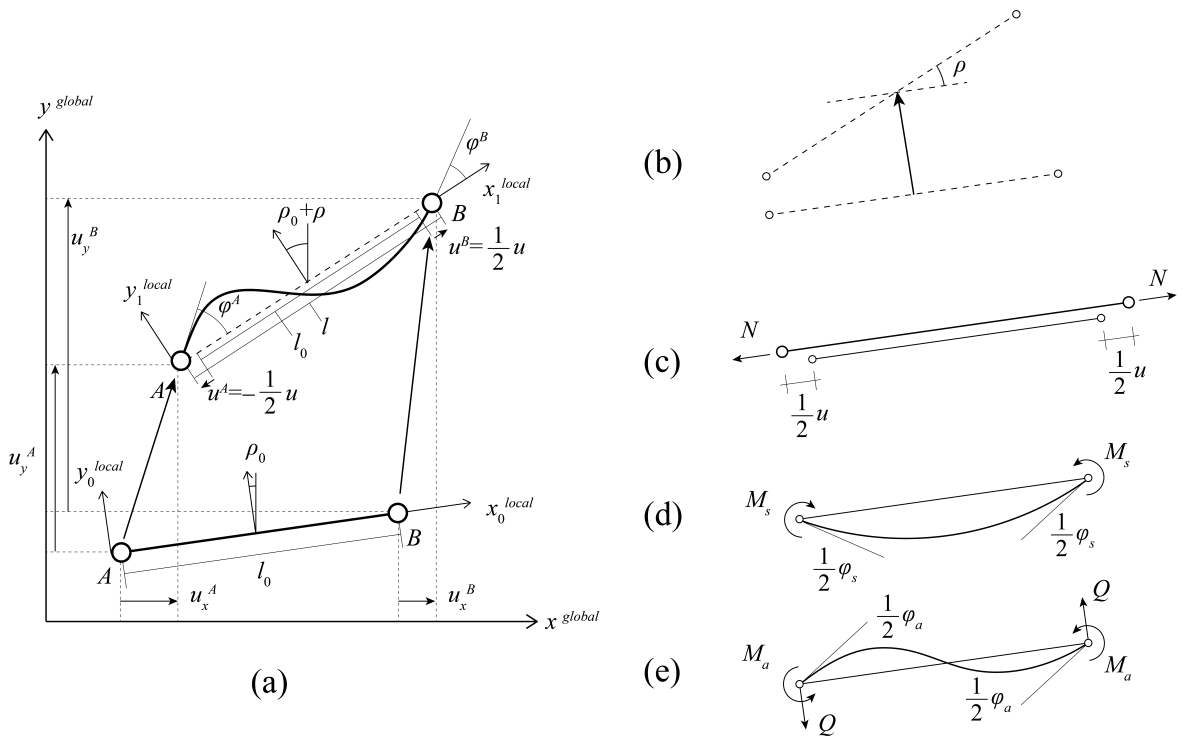


**Figure 2**: Deformation of a 2-dimensional beam element; (a) motion of beam element in global and element coordinate systems, (b) rigid body mode: translation and rotation, (c) axial extension, (d) symmetric bending, (e) anti-symmetric bending.

the co-rotational coordinate system are formulated as

$$\mathbf{p}_e = \mathbf{S}\mathbf{v} \quad \text{and} \quad \mathbf{q}_e = \mathbf{S}\mathbf{t} \quad \text{with} \quad \mathbf{S} = \begin{bmatrix} \mathbf{S}_1 \\ \mathbf{S}_2 \end{bmatrix} = \begin{bmatrix} -1 & 0 & 0 \\ 0 & 0 & 2/l \\ 0 & -1 & 1 \\ 1 & 0 & 0 \\ 0 & 0 & -2/l \\ 0 & 1 & 1 \end{bmatrix}, \tag{1}$$

where $\mathbf{S}$ and $l$ denote transformation matrix and the current length of a beam, respectively. We also introduce the transformation from displacements $\mathbf{p}_g$ and forces $\mathbf{q}_g$ in the global coordinate system to $\mathbf{p}_e$ and $\mathbf{q}_e$ by using a matrix $\mathbf{R}_e$ as follows:

$$\mathbf{p}_g = \mathbf{R}_e\mathbf{p}_e = \mathbf{R}_e\mathbf{S}\mathbf{v} \quad \text{and} \quad \mathbf{q}_g = \mathbf{R}_e\mathbf{q}_e = \mathbf{R}_e\mathbf{S}\mathbf{t}, \tag{2}$$

where $\mathbf{R}_e$ is expressed as a combined form with respect to the rotation matrix $\mathbf{R}$ and written by

$$\mathbf{R}_e = \begin{bmatrix} \mathbf{R} & \\ & \mathbf{R} \end{bmatrix} \quad \text{with} \quad \mathbf{R} = \begin{bmatrix} \cos\rho & -\sin\rho & 0 \\ \sin\rho & \cos\rho & 0 \\ 0 & 0 & 1 \end{bmatrix}, \tag{3}$$

where ρ denotes the rotation between the initial and current axes of a beam. Equations (1)–(3) represent the transformation between global and co-rotational coordinate systems.

To carry out the gradient-based simulation e.g. Newton-Raphson method, the global coordinate tangent stiffness $\mathbf{K}_g$ is derived from the co-rotational tangent stiffness $\mathbf{K}_d = \frac{\partial \mathbf{t}}{\partial \mathbf{v}}$ via the coordinate transformations. Note that the element stiffness matrix $\mathbf{K}_e$ is divided into the following two terms:

$$\mathbf{K}_e = \mathbf{S}\mathbf{K}_d\mathbf{S}^{\mathrm{T}} + \mathbf{K}_r. \tag{4}$$

The second term $\mathbf{K}_r$ is computed by

$$\mathbf{K}_r = \begin{bmatrix} \mathbf{K}^r_{11} & \mathbf{K}^r_{12} \\ \mathbf{K}^r_{21} & \mathbf{K}^r_{22} \end{bmatrix} \quad \text{with} \quad \mathbf{K}^r_{11} = \mathbf{K}^r_{22} = -\mathbf{K}^r_{12} = -\mathbf{K}^r_{21} = \frac{1}{l}\begin{bmatrix} 0 & -Q & 0 \\ -Q & N & 0 \\ 0 & 0 & 0 \end{bmatrix}, \tag{5}$$

where $Q(=-2M_a/l)$ represents shear force complementing the equilibrium system in the anti-symmetric bending mode of a co-rotational beam element. The global coordinate tangent stiffness matrix $\mathbf{K}_g$ is finally computed by using the element stiffness matrix $\mathbf{K}_e$ and rotational transformation matrix $\mathbf{R}_e$ as

$$\mathbf{K}_g = \mathbf{R}_e\mathbf{K}_e\mathbf{R}_e^{\mathrm{T}}. \tag{6}$$

## 3 GENERATION OF DATASETS

In this section, we explain how to generate the datasets used for training our surrogate models for predicting in-plane deformations of a compliant mechanism. The procedure for generating the datasets is divided into the following three steps: (i) generate $n$ random samples of $\mathbf{t}$ with the Latin hypercube sampling (LHS) method, (ii) carry out large-deformation analyses, corresponding to $n$ sampled datasets of $\mathbf{t}$, of a compliant mechanism composed of multiple beams under the boundary condition as shown in Fig. 3, and (iii) store the datasets consist of pairs of the co-rotational coordinate strains $\mathbf{v}$ and stresses $\mathbf{t}$, which are derived from the displacements and forces at both ends of a compliant mechanism, respectively, as follows:

$$\mathbf{v} = \begin{bmatrix} u \\ \varphi^B - \varphi^A \\ \varphi^A + \varphi^B \end{bmatrix} \quad \text{and} \quad \mathbf{t} = \begin{bmatrix} N \\ M^B - M^A \\ M^A + M^B \end{bmatrix}, \tag{7}$$

where $N$, $M^A$, and $M^B$ denote external force and moments applied to node A and B, respectively, as illustrated in Fig. 3(a); $u$, $\varphi^A$, and $\varphi^B$ denote translation at node B and rotations at nodes A and B, respectively, as illustrated in Fig. 3(b). Note that node A of a detail model has a pin-support and node B is roller-supported that can move along X-direction.

We apply external forces instead of forced displacements to end nodes of a detail model for sampling datasets, because multiple deformed equilibrium states can be obtained by bifurcation of the deformation-path, which means that it is unfavorable to construct a surrogate model due to the noise. To overcome the problem due to bifurcation, the Newton-Raphson method is used for solving the numerical simulation, because we can eliminate the 'ill' datasets, which cause the disturbance such as steepness on the whole datasets, by utilizing the divergence of the simulations.

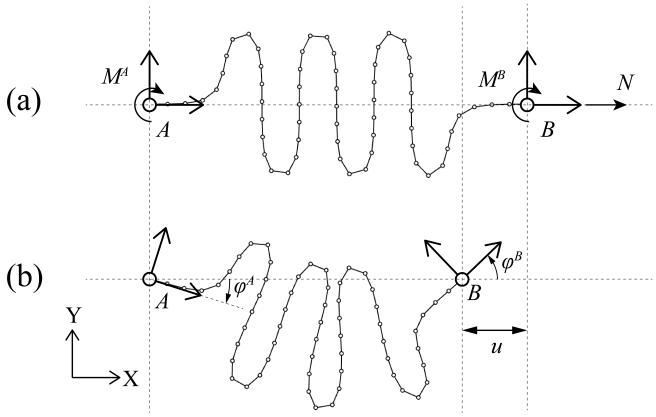


**Figure 3**: Boundary condition given to a detail model for generating datasets; (a) initial state, (b) deformed equilibrium state.

## 4 SURROGATE MODELS

Surrogate model is appropriate for expressing approximately a highly complex function of disordered (scattered) datasets, which are difficult to be represented in any analytical form. Constructing a surrogate model corresponds to finding a feasible set of hyperparameters determined by minimizing the errors between the target and prediction outputs. It is crucial to use a differentiable function as a basis function of surrogate model, because its derivatives are required to find a feasible solution for the optimization problem minimizing the errors. We construct three surrogate models: polynomial approximation, radial basis function (RBF), and neural network (NN), because they are typical learning algorithms for estimating a nonlinear function and have been used for solving a wide range of engineering problems. Note that input and output used for learning of our surrogate models are strains and stresses, respectively.

### 4.1 Polynomial approximation

The nonlinear response $\mathbf{t}(\mathbf{v})$ of a single equivalent beam element is estimated by using polynomial approximation. Based on a constitutive equation of a co-rotational beam element, the $\Xi$-dimensional Taylor expansion of $\mathbf{t}(\mathbf{v})$ has the following canonical expression:

$$\mathbf{t}(\mathbf{v}) = \sum_{\xi=1}^{\Xi} \mathbf{K}_\xi \mathbf{v}_\xi, \tag{8}$$

where $\mathbf{K}_\xi \in \mathbb{R}^{3\times {}_3\mathrm{H}_\xi}$ denotes stiffness matrix corresponding to the $\xi$th term. Letting $h.o.t$ stand for higher order terms, Eq. (8) is rewritten by using the components of $\mathbf{v}_\xi$ as

$$\begin{aligned}\mathbf{t}(\mathbf{v}) =& \mathbf{K}_1 \left[u, \varphi_s, \varphi_a\right]^{\mathrm{T}} + \mathbf{K}_2 \left[u^2, {\varphi_s}^2, {\varphi_a}^2, u\varphi_s, u\varphi_a, \varphi_s, u\varphi_a\right]^{\mathrm{T}} \\ &+ \mathbf{K}_3 \left[u^3, {\varphi_s}^3, {\varphi_a}^3, u^2\varphi_s, u^2\varphi_a, u{\varphi_s}^2, u{\varphi_a}^2, {\varphi_s}^2\varphi_a, \varphi_s{\varphi_a}^2, u\varphi_s\varphi_a\right]^{\mathrm{T}} + h.o.t.\end{aligned} \tag{9}$$

The total dimension $\Xi$ of our polynomial approximation is specified as the value, where the best prediction performance is obtained, in the range of $1 \leq \Xi \leq 10$.

### 4.2 Radial basis function

In a wide range of engineering problems, the RBF has been generally used as an approximation for estimating a response surface for large scattered datasets [5]. The basic idea of this approach is to generate the response surface as a linear combination composed of multiplications of weights and RBF. The obtained response surface passes on the target datasets. The basis function $\phi(\mathbf{x},\mathbf{c})$ with respect to an input variable $\mathbf{x}$ is defined as a real function depending on the distance from the RBF center $\mathbf{c}$ to $\mathbf{x}$. A general form of $\phi(\mathbf{x},\mathbf{c})$ can be described by $\phi(\mathbf{x},\mathbf{c}) = \phi(||\mathbf{x}-\mathbf{c}||)$. We use Gaussian function $\phi(\mathbf{x},\mathbf{c}) = \exp\left[-\varepsilon(||\mathbf{x}-\mathbf{c}||)^2\right]$ as RBF, where $\varepsilon$ is the hyperparameter defined as the 'influence' of a single training data on all datasets. Here, RBF centers $\mathbf{c}$ are $k_{\max}$ strains $\mathbf{v}_1,\ldots,\mathbf{v}_{k_{\max}}$ sampled from the generation of datasets. The interpolation function is written by the following linear combination:

$$f(\mathbf{v}) = \sum_{k=1}^{k_{\max}} w_k \phi(||\mathbf{v}-\mathbf{v}_k||), \tag{10}$$

where $w_k$ is the RBF weights on the $k$th relationship between the input and output. To find a feasible set of the components of weight vector $\mathbf{w} = [w_1,\ldots,w_{k\max}]$, the interpolation function satisfies the condition $f(\mathbf{v}_k) = \mathbf{t}_k$ for the $k$th dataset. We finally obtain the RBF weights $\mathbf{w}$ by carrying out least squared method for minimizing the differences $||f(\mathbf{v}_k)-\mathbf{t}||$ for all $k$.

### 4.3 Neural network

NN, an artificial network model inspired by a combination of biological neurons [6], can be utilized as a surrogate model for predicting nonlinear responses of large-deformation behaviors of an elastic beam model [3]. We use multilayer perception (MLP), which is a general form of NNs and consists of fully connected multiple layers composed of units. The network constructed in this paper has a single hidden layer following a classical MLP, and the hidden layer has 50 units, as shown in Fig. 4. The units in the

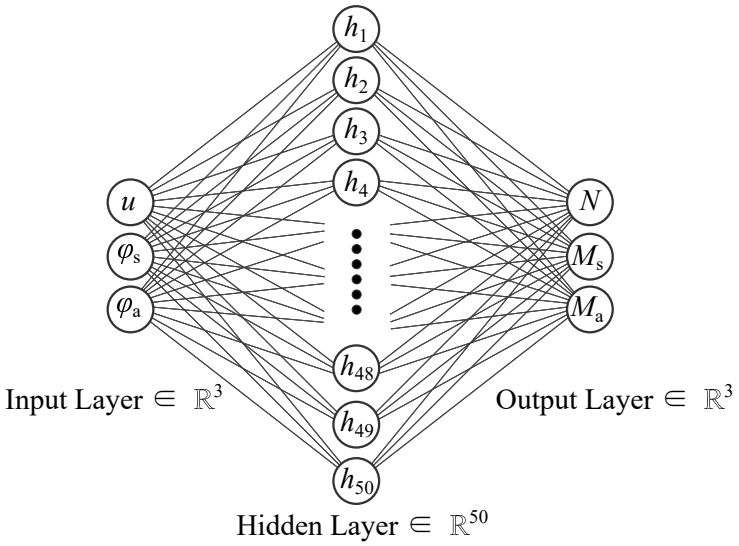


**Figure 4**: Architecture of our NN based on a classical MLP with one hidden layer composed of 50 units.

hidden layer denoted by $h_m$; $m = 1, \ldots, 50$ are computed as

$$h_m = \sigma\left(\sum_{l=1}^{3} w_{ml}^{(1)} v_l + b_m^{(1)}\right), \tag{11}$$

where $\sigma(\cdot)$, $w_{ml}^{(1)}$, and $b_m^{(1)}$ denote activation function, weight parameters, and bias parameters, respectively. Superscript (1) in Eq. (11) indicates that the parameters consist of the first layer of our NN. We choose the logistic sigmoid function $1/(1+e^{-v})$, which is differentiable, as $\sigma(\cdot)$ for all connections between the units in two neighboring layers. The units in the output layer are written by

$$t_l(\mathbf{v}, \mathbf{w}, \mathbf{b}) = \sigma\left(\sum_{m=1}^{50} w_{lm}^{(2)} \sigma\left(\sum_{l=1}^{3} w_{ml}^{(1)} v_l + b_m^{(1)}\right) + b_l^{(2)}\right), \tag{12}$$

where $\mathbf{w}$ and $\mathbf{b}$ represent vectors composed of weight and bias parameters, respectively.

The learning process of NN is classified into two phases: the training and test phases. We randomly assign 90% of datasets to the training phase and 10% to the test one. During the training phase, the loss function defined as mean squared error $\sum_{k=1}^{k_{\max}} ||\mathbf{t}_k - \hat{\mathbf{t}}_k||^2 / k_{\max}$ is minimized based on error backpropagation, which is a computational procedure to obtain the partial derivatives of predictions with respect to variables from outputs to inputs. $k_{\max}$ is the number of datasets collected by large-deformation analysis with the detail model composed of multiple beam elements, and $\mathbf{t}_k$ and $\hat{\mathbf{t}}_k$ represent the $k$th target and prediction outputs, respectively. We choose the batch size equal to the total number of datasets; batch learning is performed. Optimization is therefore carried out via gradient descent. Learning rate is 0.0001. Training our NN is performed until 500000 epochs. The set of hyperparameters is determined manually by trial and error. We use PyTorch [7], a Python library of NN, for constructing the architecture of our NN and carrying out the learning process.

## 5 RESULTS

To investigate the prediction performances of the three surrogate models as introduced in Sec. 4, we carry out the training and test of scattered datasets for nonlinear responses between strains $\mathbf{v}$ and stresses $\mathbf{t}$ of four types of compliant mechanisms: Simple beam, Kazaguruma, Spiral, and Rhombus. The numbers of datasets for Simple beam, Kazaguruma, Spiral, and Rhombus are 1000, 1000, 487, and 1000, respectively. Note that we eliminate the datasets not converged in the numerical simulations with the detail model of Spiral.

By carrying out standardization, a statistical procedure to tune the variables of datasets, the mean is set as 0 and standard deviation 1 for each variable. To eliminate the deterioration of the performances due to the different scales and types of variables, standardization is to be carried out prior to the learning process. Computation is carried out on a PC with Intel Core i7-9750H 4.50 GHz, 32.0GB RAM, and six cores.

### 5.1 Comparison of our surrogate model predictions

In the following examples, we use a material with Young's modulus 300 MPa and Poisson's ratio 0.3. The beam has a rectangle section with width 2 mm and height 4 mm. The initial length of each beam element is 100 mm. We investigate the following average differences between the numerical simulation results with detail models and the surrogate model predictions: (i) distance of vectors $\mathbf{t} = [N, M_s, M_a]^{\mathrm{T}} =$

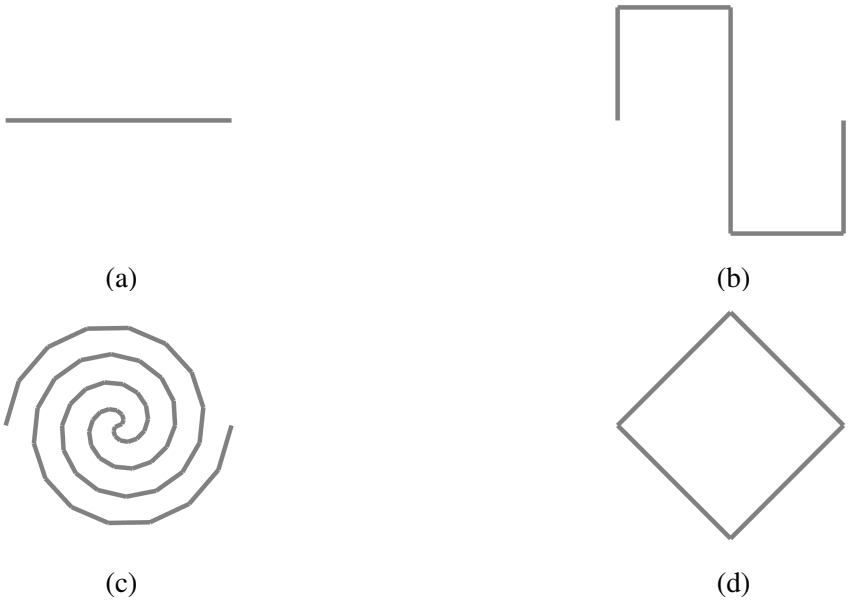


**Figure 5**: Geometrical configurations of compliant mechanisms used for investigation of prediction performances of our surrogate models; (a) Simple beam, (b) Kazaguruma, (c) Spiral, (d) Rhombus.

$[t_1,t_2,t_3]^{\mathrm{T}}$ and $\hat{\mathbf{t}} = [\hat{N},\hat{M}_s,\hat{M}_a]^{\mathrm{T}} = [\hat{t}_1,\hat{t}_2,\hat{t}_3]^{\mathrm{T}}$, (ii) axial stresses, (iii) symmetric bending stresses, and (iv) anti-symmetric bending stresses, which are defined as

$$\frac{1}{k_{\max}}\sum_{k=1}^{k_{\max}}\frac{||\mathbf{t}_k-\hat{\mathbf{t}}_k||}{||\mathbf{t}_k||}\times 100\ \ (\%)\quad\text{and}\quad\frac{1}{k_{\max}}\sum_{k=1}^{k_{\max}}\frac{|t_{lk}-\hat{t}_{lk}|}{|t_{lk}|}\times 100\ \ (\%) \tag{13}$$

with $l \in \{1,2,3\}$.

Table 1 shows the average differences of forces at both ends of the detail model and the equivalent beam model based on our surrogate models. For all compliant mechanisms, the polynomial approximation and NN are not performed better than our RBF. Our trained RBF can produce good prediction performances of the numerical simulation with the detail models. The average differences obtained from our RBF for all compliant mechanisms are lower than 1%. Notably, the prediction performances of RBF constructed for Rhombus are good, and the average differences of the force vector and its components are lower than $1.0\times10^{-3}\%$. As seen in the results, the in-plane nonlinear structural responses of the four compliant mechanisms can be predicted practically by our RBF.

### 5.2 Comparison of computational time of detail and surrogate models

We compare the computational time of numerical simulations with the detail model and prediction with our RBF. Three compliant mechanisms, whose initial shapes are straight and composed of single, five, and ten Spirals, are set to serve as our benchmark. We set ten random cases of boundary conditions applied to both ends of the compliant mechanisms, and measure the average computational time required for a convergence of a numerical simulation.

The average times of the detail model and our RBF are 116.2 ms and 7.5 ms for single, 7278.2 ms and 45.7 ms for five, 86358 ms and 227.4 ms for ten Spirals, respectively. The large-deformation analyses for

**Table 1**: Average differences between the numerical simulation results with detail models and our surrogate model predictions for nonlinear structural responses of four types of compliant mechanisms.

| (unit: %) | | Polynomial approximation | RBF | NN |
|---|---|---|---|---|
| Simple beam | $\mathbf{t}$ | 1.5150 | 0.0022 | 0.1891 |
| | $N$ | 10.553 | 0.0505 | 2.0564 |
| | $M_s$ | 0.8086 | 0.0009 | 0.4382 |
| | $M_a$ | 0.1281 | 0.0002 | 1.1381 |
| Kazaguruma | $\mathbf{t}$ | 0.7994 | 0.0010 | 0.1483 |
| | $N$ | 0.2562 | 0.0067 | 0.2365 |
| | $M_s$ | 0.9572 | 0.0012 | 0.3847 |
| | $M_a$ | 3.3246 | 0.0029 | 0.7026 |
| Rhombus | $\mathbf{t}$ | 0.0007 | 0.00003 | 0.0124 |
| | $N$ | 0.0065 | 0.0002 | 0.0380 |
| | $M_s$ | 0.0012 | 0.00003 | 0.0575 |
| | $M_a$ | 0.0005 | 0.0002 | 0.0263 |
| Spiral | $\mathbf{t}$ | 0.2684 | 0.0003 | 0.1311 |
| | $N$ | 0.1090 | 0.0002 | 0.1050 |
| | $M_s$ | 0.8005 | 0.0010 | 0.2636 |
| | $M_a$ | 0.3026 | 0.0004 | 0.2405 |

single, five, and ten Spirals are approximately 16, 160, and 380 times faster using the equivalent beam model based on our trained RBF than the detail model, respectively.

### 5.3 Prediction of in-plane deformation behavior of compliant mechanisms composed of multiple Spirals

We further validate the proposed surrogate model in two numerical examples: Straight model and Grid model. Our RBF trained with a single Spiral is implemented for predicting in-plane deformation behaviors of the examples.

Figure 6 shows the initial and deformed shapes of the detail models composed of multiple beam members and the equivalent beam models based on our RBF for predicting the deformation behaviors of Spiral. The geometrical configurations of the detail models are illustrated by black piecewise linear curves, and the equivalent beam models blue lines. Straight model, which is unstressed in the initial state, is arranged along $x$-axis. The detail model has five Spirals, pin-supported at one end, and roller-supported at the other end allowing translational displacement in $x$-direction. The equivalent beam model has six nodes, and the boundary conditions are equivalent to the detail one. We apply external forces of $-0.0033$ N along the axial direction and symmetric and anti-symmetric moments of 0.21107 Nmm and 0.026528 Nmm at both ends of the model, respectively.

Grid model has $200 \times 200$ (mm) square boundary and four internal Spirals intersecting at the center. The detail model is composed of twelve Spirals, and the equivalent beam model has twelve co-rotational beam elements arranged in the grid. The three nodes in the left column are fixed, and the others can move in $xy$-plane. Forced displacements of 100 mm are applied at the node connecting the two Spirals in the right column towards the opposite direction of the center node of the grid.

As seen in Figure 6(b), we can see that the coordinates of all nodes between the detail and equiv-

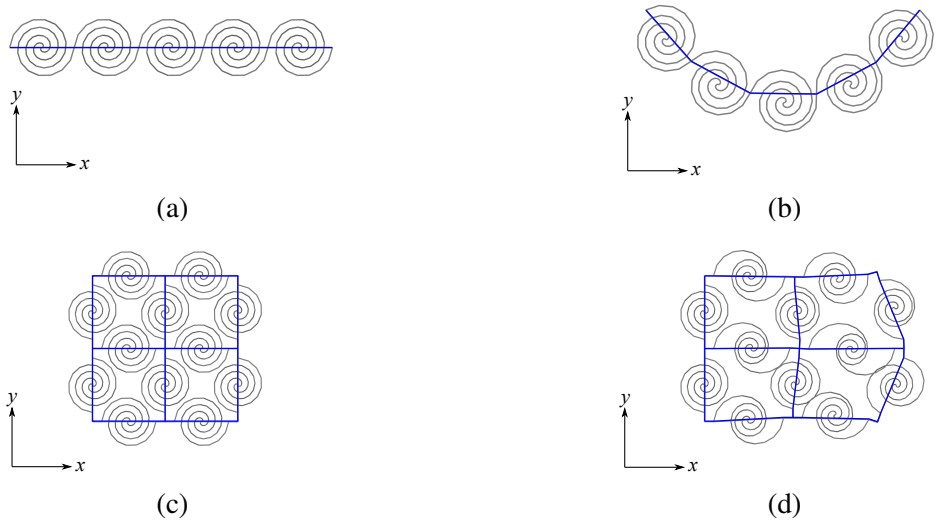


**Figure 6**: Initial and deformed shapes of compliant mechanisms with multiple Spirals. (Grey) Detail model. (Blue) Equivalent beam element based on our RBF; (a) initial shape of Straight model, (b) deformed shape of Straight model, (c) initial shape of Grid model, (d) deformed shape of Grid model.

alent beam models of Straight model are almost the same. The average and maximum differences in $x$-direction are 0.0056 mm and 0.0099 mm, respectively, and those in $y$-direction are 0.0026 mm and 0.0059 mm, respectively. The differences are sufficiently small for the total length of Straight model.

Also, Fig. 6(d) shows that the coordinates of all nodes between the detail and surrogate models of Grid model are very close. The average and maximum differences in $x$-direction are 0.1055 mm and 0.7906 mm, respectively, and those in $y$-direction are 0.0844 mm and 0.3710 mm, respectively. Although the differences for Grid model are larger than those for Straight model, they are small for practical use of the proposed model for finding better candidate solutions.

## 6 CONCLUSIONS

The main purpose of this paper is to propose a surrogate model for predicting nonlinear deformation behaviors of a compliant mechanism. We use a 2-dimensional co-rotational beam element, with the three essential deformation DOFs, for reducing computational costs of large-deformation analysis of a detail model composed of bending beams, with six DOFs at each end. This procedure can degenerate the dimensions of inputs and outputs, from six to three, used for training our surrogate models. The datasets used for constructing the surrogate models are firstly sampled as forces and displacements by carrying out the numerical simulation by finite-element method with the detail model, and they are converted into stresses and strains associated with the three essential deformation DOFs in the co-rotational coordinate system. We adopt the LHS method for generating random sets of forces applied to both ends of the detail model. Note that the forces and displacements at both ends of the detail model correspond to inputs and outputs for the sampling datasets, respectively; however, the co-rotational coordinate strains and stresses correspond to inputs and outputs for constructing a surrogate model, respectively. In the numerical example, we investigate the prediction performances of the constructed surrogate models for the four

types of compliant mechanisms: Simple beam, Kazaguruma, Spiral, and Rhombus. Comparing the differences of the target and prediction outputs, the results show that our RBF exhibits better prediction performances than our polynomial approximation and NN. Notably, our RBF has great performance for predicting in-plane deformation behaviors of Spiral and Rhombus. To validate that our surrogate models enable us to resolve high computational costs for carrying out large-deformation analysis with the geometrical nonlinearities, we measure the computational time of the detail model and our RBF for the different sizes of Spirals. As a result, the use of our RBF for Spiral can significantly reduce computational costs. Furthermore, the average differences of coordinates of all nodes between the detail model and our RBF for Straight and Grid models are sufficiently small. The results suggest that our surrogate model can be an alternative solver for obtaining candidate in-plane deformation behaviors of a compliant mechanism.

## REFERENCES


[1] Howell, L.L. *Compliant Mechanisms*. Wiley, (2001).

[2] Malomo, L., P'erez, J., Iarussi, E., Pietroni, N., Miguel, E., Cignoni, P. and Bickel, B. FlexMaps: Computational design of flat flexible shells for shaping 3D objects. *ACM Trans. on Graphics-Siggraph Asia 2018* (2018) **37**: 6–14.

[3] Papadopoulos, V., Soimiris, G., Giovanis, D.G. and Papadrakakis, M. A neural network-based surrogate model for carbon nanotubes with geometric nonlinearities. *Comput. Methods Appl. Mech. Engrg.* (2018) **328**: 411–430.

[4] Steen Krenk, *Non-linear Modeling and Analysis of Solids and Structures*. Cambridge University Press, (2009).

[5] Majdisova, Z. and Skala, V. Radial basis function approximations: comparison and applications. *Applied Mathematical Modelling* (2017) **51**: 728-743.

[6] Bishop, C.M. *Neural Networks for Pattern Recognition*. Oxford University Press, (1995).

[7] Paszke, A., Gross, S., Massa, F., Lerer, A., Bradbury, J., Chanan, G., Killeen, T., Lin, Z., Gimelshein, N., Antiga, L., Desmaison, A., Kopf, A., Yang, E., DeVito, Z., Raison, M., Tejani, A., Chilamkurthy, S., Steiner, B., Fang, L., Bai, J. and Chintala, S. Pytorch: An imperative style, high-performance deep learning library. *In: NeurIPS* (2019).